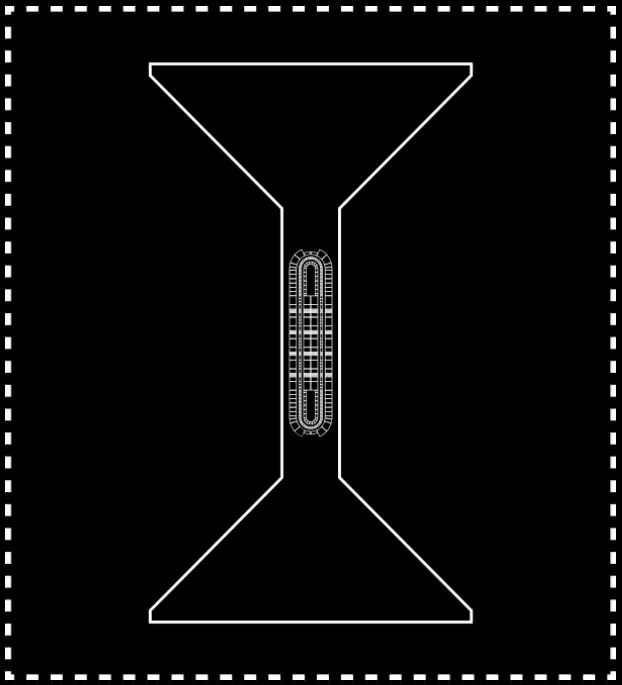

Quantinuum System Model H2

Product Data Sheet

Version 1.10   June 15, 2023

TABLE OF CONTENTS

INTRODUCTION

This Product Data Sheet covers all features and characteristics of the **Quantinuum System Model H2, Powered by Honeywell.**

FEATURES

- N ≥ 32 qubit trapped-ion based quantum computers
- All-to-all connectivity
- Laser based quantum gates
- Quantum charge-coupled device (QCCD) architecture with four (or more) gate zones in a trap consisting of two connected linear sections
- Mid-circuit measurement conditioned circuit branching
- Qubit reuse after mid-circuit measurement
- Native gate set: single-qubit rotations, two-qubit ZZ-gates, arbitrary-angle ZZ gates

SPECIFICATIONS

Table 1 lists the specifications for Quantinuum H2-1 quantum computer.

Table 1 Quantinuum System Model H2 Specifications

System Fundamentals	H2-1		
Parameters	**min**	**typ**	**max**
General			
Qubits	32		
Connectivity	All-to-all		
Parallel two-qubit operations	4		
Errors			
Single-qubit gate infidelity	1×10^{-5}	3×10^{-5}	2×10^{-4}
Two-qubit gate infidelity	1.8×10^{-3}	2×10^{-3}	5×10^{-3}
State preparation and measurement (SPAM) error	1×10^{-3}	2×10^{-3}	5×10^{-3}
Memory error per qubit at average depth-1 circuit	2×10^{-4}	6×10^{-4}	2×10^{-3}
Mid-circuit measurement cross-talk error	1×10^{-6}	5×10^{-5}	2×10^{-4}

SYSTEM OPERATION

The **Quantinuum System Model H2, Powered by Honeywell**, operates on qubits implemented through atomic hyperfine states of $^{171}Yb^{+}$. The H2 system includes 1 machine, the H2-1, which has 32 physical qubits (ions) that move, individually or in pairs, between four interaction zones where all quantum operations (initialization, measurement, single-, and two-qubit gates) are performed using lasers. By rearranging the physical location of the qubits, a two-qubit gate can be performed on any arbitrary pair, giving the system all-to-all connectivity. Additionally, because there are multiple interaction zones, multiple quantum operations may be performed in parallel.

Although the qubits are all identical, there may be differences in the errors associated with quantum operations depending on the location, i.e., interaction zone, in which the quantum operations take place, independent of the specific qubits that are in that location. However, the location for each quantum operation is determined by the compiler and may vary even for similar circuits, as each circuit is optimized to minimize the number of transport operations and the time required to run the circuit. The typical infidelities reported on this product data sheet are an average over all operational zones, with the minimum and maximum spanning both the difference between zones and the day-to-day variation.

Generational Hardware Nomenclature

System Model H2 refers to a generation of quantum computing hardware using ion traps with two connected linear sections in a racetrack geometry. Individual machines that use this generation of ion traps are designated by the H2-X nomenclature.

API Interface

Communication with Quantinuum System Model H2 occurs through an API endpoint based on the OpenQASM 2.0 standard [1]. Interface details are given in the *Quantinuum Application Programming Interface (API) Specification.*

Native Gate Set

The Quantinuum System Model H2 utilizes the following native gate set.

Native single-qubit gates:

$$U_{1q}(\theta,\varphi) = e^{-i\,(\cos\varphi\hat{X}+\sin\varphi\hat{Y})\,\theta/2} = \begin{pmatrix} \cos\frac{\theta}{2} & -ie^{-i\varphi}\sin\frac{\theta}{2} \\ -ie^{i\varphi}\sin\frac{\theta}{2} & \cos\frac{\theta}{2} \end{pmatrix}$$

$$R_z(\lambda) = e^{-i\,\hat{Z}\,\lambda/2} = \begin{pmatrix} e^{-i\,\lambda/2} & 0 \\ 0 & e^{i\,\lambda/2} \end{pmatrix}$$

Fully entangling two-qubit gate:

$$ZZ() = e^{-i\frac{\pi}{4}\hat{Z}\otimes\hat{Z}} = e^{-\frac{i\pi}{4}}\begin{pmatrix} 1 & 0 & 0 & 0 \\ 0 & i & 0 & 0 \\ 0 & 0 & i & 0 \\ 0 & 0 & 0 & 1 \end{pmatrix}$$

Arbitrary angle two-qubit gate: $RZZ(\theta) = e^{-i\frac{\theta}{2}\hat{Z}\otimes\hat{Z}} = e^{-\frac{i\theta}{2}}\begin{pmatrix} 1 & 0 & 0 & 0 \\ 0 & e^{i\theta} & 0 & 0 \\ 0 & 0 & e^{i\theta} & 0 \\ 0 & 0 & 0 & 1 \end{pmatrix}$

$$RZZ\left(\frac{\pi}{2}\right) = ZZ()$$

$\hat{X}$, $\hat{Y}$, and $\hat{Z}$ are the standard Pauli operators, and the two-qubit matrix is written in the $|0{,}0\rangle, |0{,}1\rangle, |1{,}0\rangle, |1{,}1\rangle$ basis.

It is important to note that the arbitrary rotation around the z axis, $R_z(\lambda)$, is performed virtually within the software. All other gates are constructed from this set.

*Please note that our native $U_{1q}(\theta,\varphi)$ gate is **NOT** IBM's standard $U(\theta,\varphi,\lambda)$ as defined in* [1].

$$U_{1q}(\theta,\varphi) = U\left(\theta, \varphi - \frac{\pi}{2}, \frac{\pi}{2} - \varphi\right)$$

Constructed gate examples using QASM notation

Examples using the native gate set within QASM are below.

Pauli gate: bit-flip	`x() a`	=	`U1q(pi,0) a;`
Pauli gate: bit and phase flip	`y() a`	=	`U1q(pi,pi/2) a;`
Pauli gate: phase flip	`z() a`	=	`Rz(pi) a;`

Clifford gate: Hadamard	`h() a`	=	`U1q(pi/2,-pi/2) a;`
			`Rz(pi) a;`

Clifford gate: CNOT	`CX() c,t`	=	`U1q(-pi/2, pi/2) t;`
			`ZZ() c, t;`
			`Rz(-pi/2) c;`
			`U1q(pi/2, pi) t;`
			`Rz(-pi/2) t;`

Pauli interaction: Z basis	`rzz(pi/4) c,t`	=	`RZZ(pi/4) c, t;`

Pauli interaction: X basis	`rxx(pi/4) c,t`	=	`U1q(pi/2, pi/2) c;`
			`U1q(pi/2, pi/2) t;`
			`RZZ(pi/4)c, t;`
			`U1q(pi/2, -pi/2) c;`
			`U1q(pi/2, -pi/2) t;`

Mid-circuit measurement and conditional operations

Due to the internal level structure of trapped-ion qubits, a mid-circuit measurement may leave the qubit in a non-computational state. All mid-circuit measurements should be followed by initialization if the qubit is to be used again in that circuit. The qubit may be prepared in the measured state by calling for a measurement followed by initialization and a measurement dependent spin-flip.

When a subset of qubits is measured in the middle of the circuit, the classical information from these measurements can be used to condition future elements of the circuit. Although, for QASM programs, the laser pulses that implement both single- and two-qubit gates are conditional, the transport operations used to rearrange the physical location of the qubits are not. The qubits will be reconfigured to allow for all gates in all branches irrespective of the mid-circuit measurement outcome. In the context of memory error and run time, the effective depth of a circuit with measurement conditioned branching includes all branches.

Inter-circuit performance validation

Jobs submitted with large shot-counts are automatically divided into appropriately sized chunks of smaller shot-counts in a method called “chunking.” Chunking ensures that system state-checks and dynamic calibrations happen at the appropriate frequency. The number of shots in a chunk is dynamically chosen by the compiler and will vary with the complexity of the circuit. A series of system checks are performed before and after each chunk. If an error is detected, any suspect results are rejected and the failed chunk shots are rerun at no additional cost. For jobs consisting of multiple chunks, the time between the start date and result date will include all of the system checks and calibrations that happened in the middle of that job and possibly chunks from other jobs in the queue.

Dynamic calibrations

The system automatically schedules and executes calibration routines. There are two types of automated calibrations: those that are executed on a predetermined time interval and those that are triggered when a drift tolerance is exceeded. Because the latter does not follow a predetermined schedule, the circuit throughput and execution time will vary due to these calibrations.

Depth-1 circuit time

We define the depth-1 circuit time as the time it takes to arbitrarily permute all qubits and perform single-qubit and two-qubit gates on all $\lfloor \frac{N}{2} \rfloor$ pairs, as shown in Figure 1,where P represents the random permutation of all qubits. Many circuits cannot be fully parallelized into a maximally dense circuit where each qubit participates in a two-qubit gate at each step of the circuit and may have shorter depth-1 circuit times as a result.

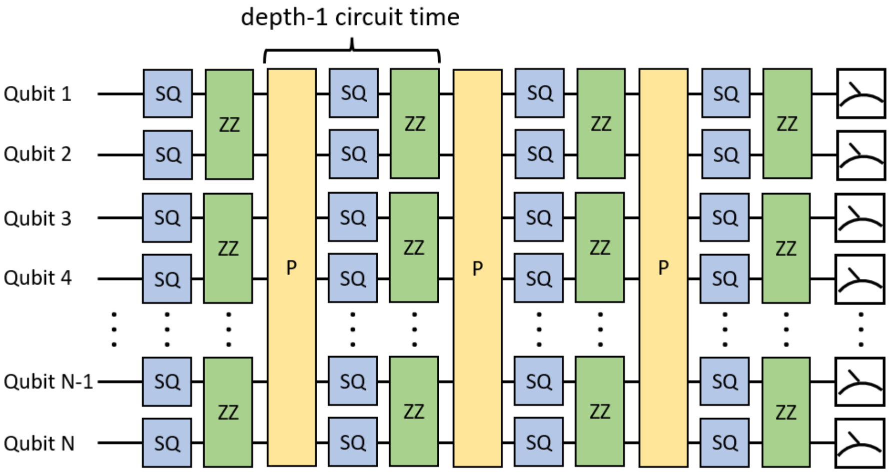

Figure 1 Depth-1 circuit time for a maximally dense circuit

Estimating circuit time

The run time for a given circuit depends on many factors, including factors in the circuit structure, such as if the circuit is highly connected or not, as well as factors in the system, such as dynamic calibrations. Run time can be reasonably predicted using the same formula that defines H-System Quantum Credits (HQC). A HQC is defined as:

$$HQC = 5 + \frac{N_{1q} + 10\, N_{2q} + 5\, N_m}{5000} C$$

where N_{1q} is the number of single-qubit gates, N_{2q} is the number of native two-qubit gates, N_m is the number of state preparation and measurement operations in a circuit, including the initial implicit state preparation and any intermediate and final measurements and resets, and C is the shot count. When a circuit is submitted, the cost in HQCs is returned with the results. For circuits using conditional logic, the charged HQCs include all the gates and measurements across all conditional branches regardless which are executed in the circuit.

Arbitrary Angle ZZ Gates

Although an abitrary angle two-qubit entagling gate can be constructed using two fixed angle two-qubit entangling gates, a direct implementation will lower the error rate in the circuit. Not only is the number of entangling gates reduced, but the error of an RZZ(θ) gate also scales with the angle θ. The error on RZZ(π/2) is equal to the error of ZZ().

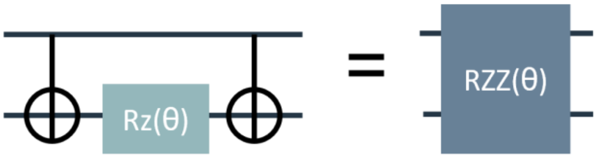

Figure 2 Quantum circuits that use the gate sequence CNOT, RZ, CNOT can be replaced with the arbitrary angle ZZ gate. This enables a lower number of two-qubit gates in a quantum circuit, improving performance by decreasing gate errors.

ERROR DEFINITIONS

Single-qubit gate fidelity

The single-qubit gate fidelity is measured using single-qubit randomized benchmarking (RB) with random single-qubit Clifford gates [2]. Benchmarking also uses final gate randomization, similar to Ref. [3], to fix the asymptote of the RB decay curve in order to reduce the number of fit parameters and allow fitting of shorter sequences. We run single-qubit RB with two qubits per active gate zone in parallel. The error rate is calculated by translating the RB decay curve to a per-Clifford average infidelity under the standard RB assumptions. Uncertainty is calculated from a semi-parametric bootstrap resampling of the collected data.

The spontaneous emission rate is also measured from single-qubit RB experiments by applying a “leakage gadget” to the end of each circuit, which detects if a qubit leaks out of the computational subspace. The number of leakage events depends on the number of gates applied and the spontaneous emission rate. By fitting the number of detected leakage events as a function of number of gates, we can extract an estimate of the spontaneous emission rate.

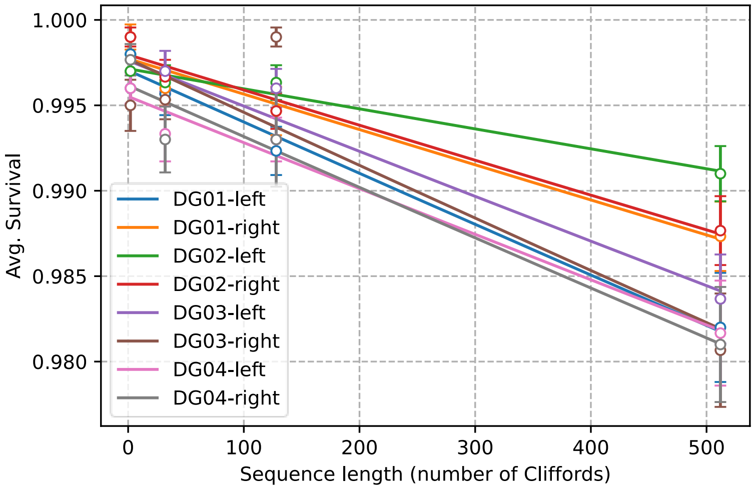

Figure 3 Single-qubit RB data from H2-1 taken on 2023/03/10.

Two-qubit gate fidelity

The two-qubit gate fidelity is measured with two-qubit RB using similar methods outlined above on single-qubit RB. Two-qubit RB is run with two-qubit random Clifford gates on pairs of qubits in each active gate zone in parallel. The infidelity of our native entangling gate is estimated by scaling per-Clifford infidelity by the average number of entangling gates per Clifford (= 1.5). Datasets also include the estimated spontaneous emission rate using the leakage gadget described above and scaled for the number of two-qubit gates per Clifford.

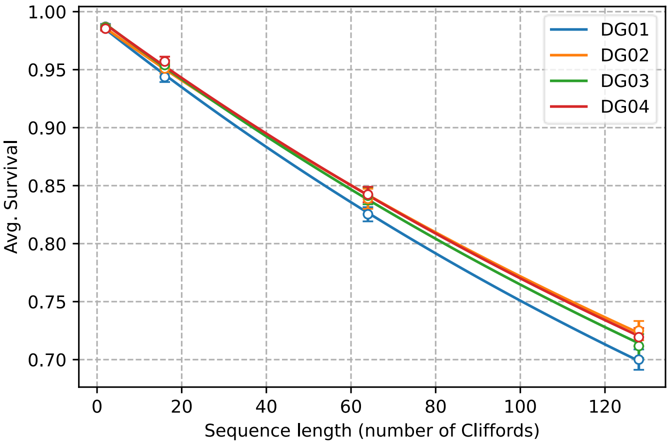

Figure 4: Two-qubit RB results from H2-1 taken on 2023/03/20.

State preparation and measurement (SPAM) error

The SPAM error is measured by preparing the qubits in the $|0\rangle$ (or $|1\rangle$) state and measuring to determine the fraction of time the incorrect $|1\rangle$ (or $|0\rangle$) state is returned. The reported SPAM error is the average between the $|0\rangle$ and $|1\rangle$ state preperation experiments. The experiment is repeated for two qubits per active gate zone and done in parallel.

Mid-circuit measurement and reset cross-talk error

Although qubits are physically separated during measurement, there is a small chance that an unmeasured qubit in the $|1\rangle$ state will absorb the detection light, destroying its quantum state, and potentially scattering to the non-computational states used for state detection. This is not an issue with measurement at the end of a circuit when all qubits are measured but can impact circuits with mid-circuit measurement and reset. The mid-circuit measurement and reset cross-talk errors are quantified by the population decay of an unmeasured qubit while applying many measurement or reset pulses to a neighboring qubit as described in Ref. [4].

Memory error per qubit at depth-1 circuit time

To characterize memory error in depth-1 circuit time, we perform single-qubit RB as described above, while interleaving specialized qasm commands that force transport to create random two-qubit pairings and run the preset cooling. The net RB error measured is the average single-qubit error due to depth-1 circuits. We perform this test for all available qubits in the system.

Benchmarking Data

The data for the measurements in this document can be found online at: https://github.com/CQCL/quantinuum-hardware-specifications. This repository contains the raw data along with the analysis code.

REFERENCES

[1] A. W. Cross, L. S. Bishop, J. A. Smolin and J. M. Gambetta, "Open Quantum Assembly Language," *arXiv:1707.03429v2,* 2017.

[2] E. Magesan, J. M. Gambetta and J. Emerson, "Characterizing quantum gates via randomized benchmarking," *Phys. Rev. A,* vol. 85, no. 4, p. 042311, 2012.

[3] R. Harper, I. Hincks, C. Ferrie, S. T. Flammia and J. J. Wallman, "Statistical analysis of randomized benchmarking," *Phys. Rev. A,* vol. 99, no. 5, p. 052350, 2019.

[4] J. P. Gaebler, C. H. Baldwin, S. A. Moses, J. M. Dreiling, C. Figgatt, M. Foss-Feig, D. Hayes and J. M. Pino, "Suppression of midcircuit measurement crosstalk errors with micromotion," *Phys. Rev. A,* vol. 104, no. 6, 2021.